Electronic Supplementary Material (ESI) for Journal of Materials Chemistry A.

Supporting Information

Modified lithium metal anode via anions-planting protection mechanisms for dendrite-free long-life lithium metal batteries

*Fulu Chu, Jie Lei, Rongyu Deng, You Zhou and Feixiang Wu**

School of Metallurgy and Environment, Engineering Research Center of the Ministry of Education for Advanced Battery Materials, Hunan Provincial Key Laboratory of Nonferrous Value-added Metallurgy, State Key Laboratory of Powder Metallurgy, Central South University, Changsha 410083, PR China

* Corresponding authors: Feixiang Wu (feixiang.wu@csu.edu.cn)

Keywords: Li metal anode, anode protection, solid electrolyte interphase, artificial SEI, salt anions

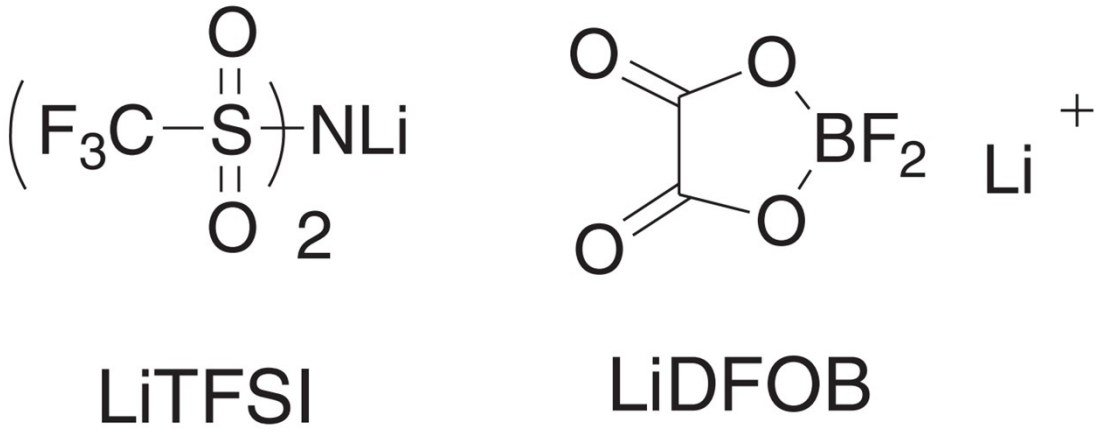

Fig. S1. The molecular structures of lithium salts[1] used in this work.

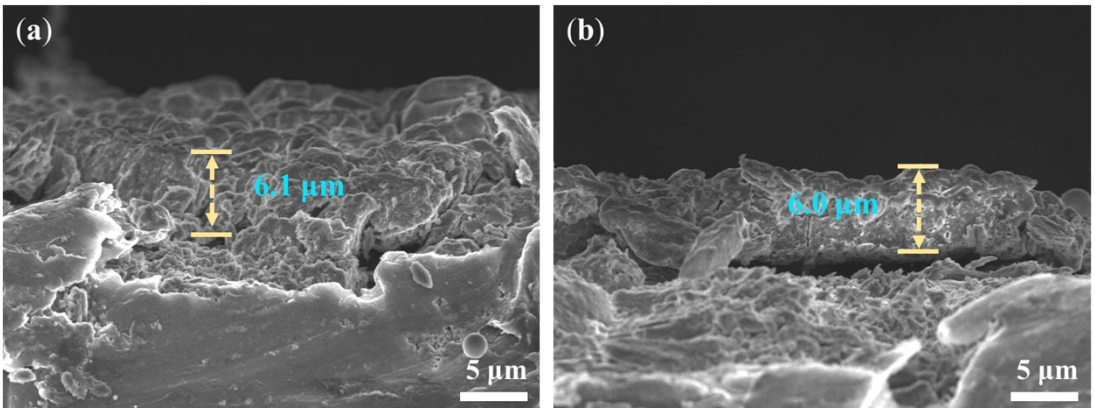

Fig. S2. The cross-sectional morphology of modified Li anode via SEM in a, b) different regions.

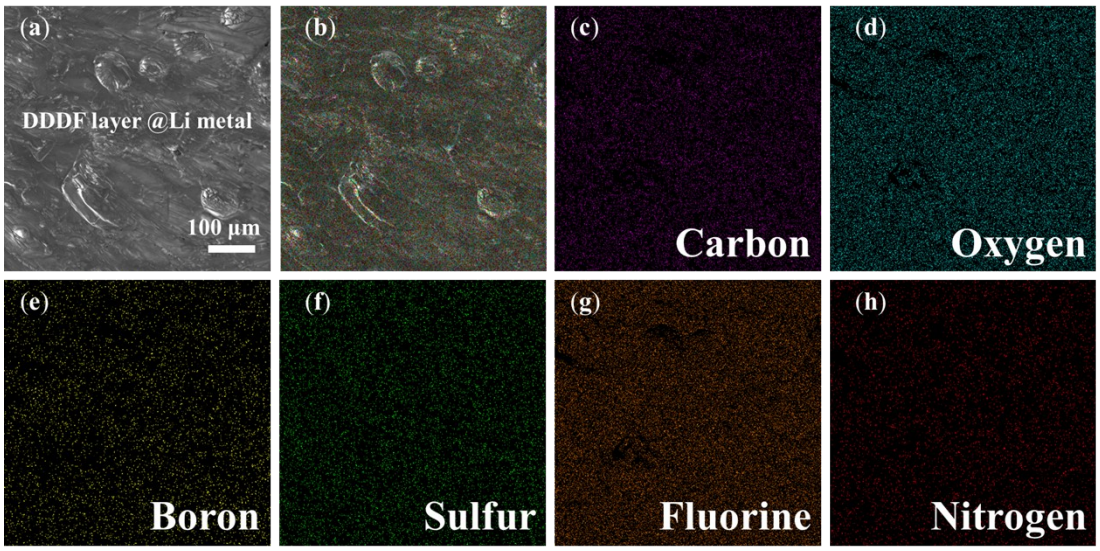

Fig. S3. (a) The morphology of modified Li anode via SEM and (b) corresponding EDS elemental maps for (c) C, (d) O, (e) B, (f) S, (g) F, and (h) N.

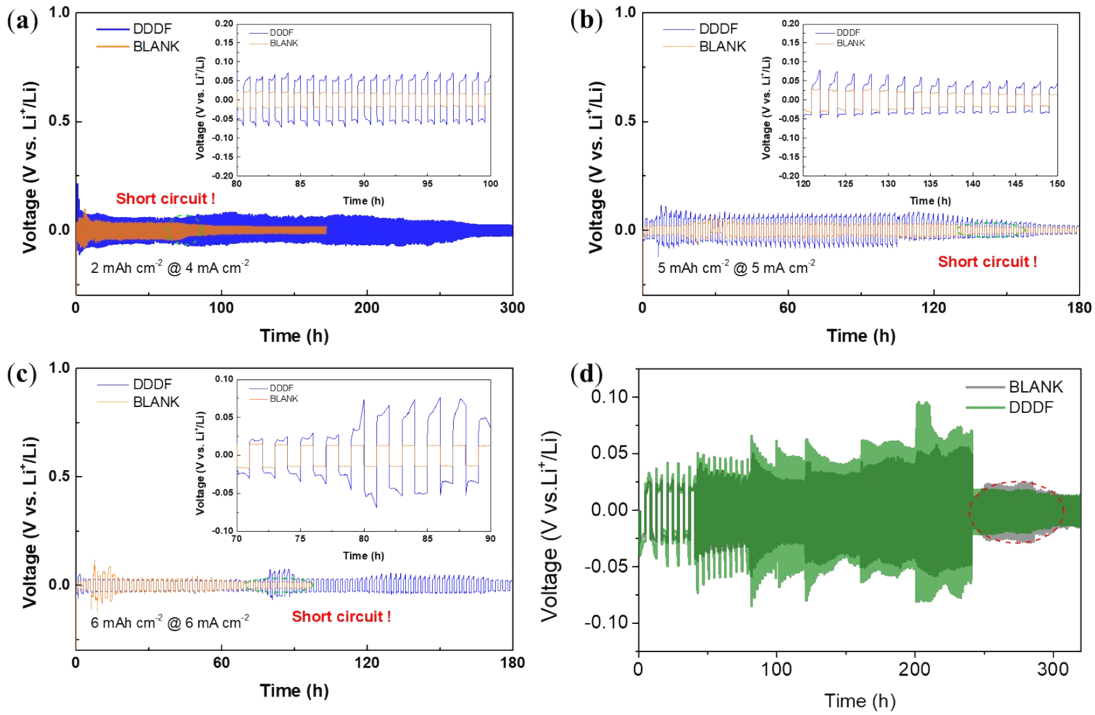

Fig. S4. Cycling performances of symmetric Li||Li cells with DDDF@Li foil at various current densities. Time–voltage profiles at (a) 4 mA cm^{-2}–0.5 h, (b) 5 mA cm^{-2}–1 h, (c) 6 mA cm^{-2}–1 h, and (d) rate test.

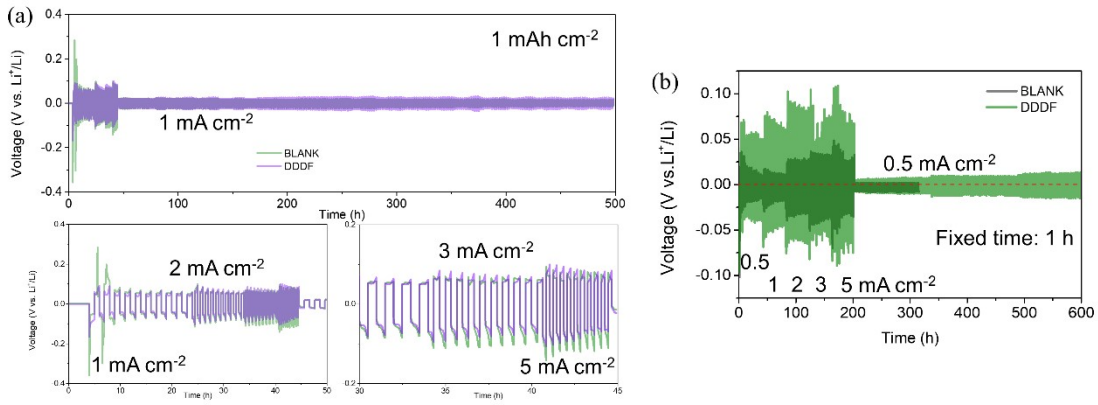

Fig. S5. Rate cycling performance of symmetric Li||Li cells with DDDF@Li foils at (a) different currents for a fixed capacity of 1 mAh cm^{-2} and (b) different currents for a fixed time of 1 h.

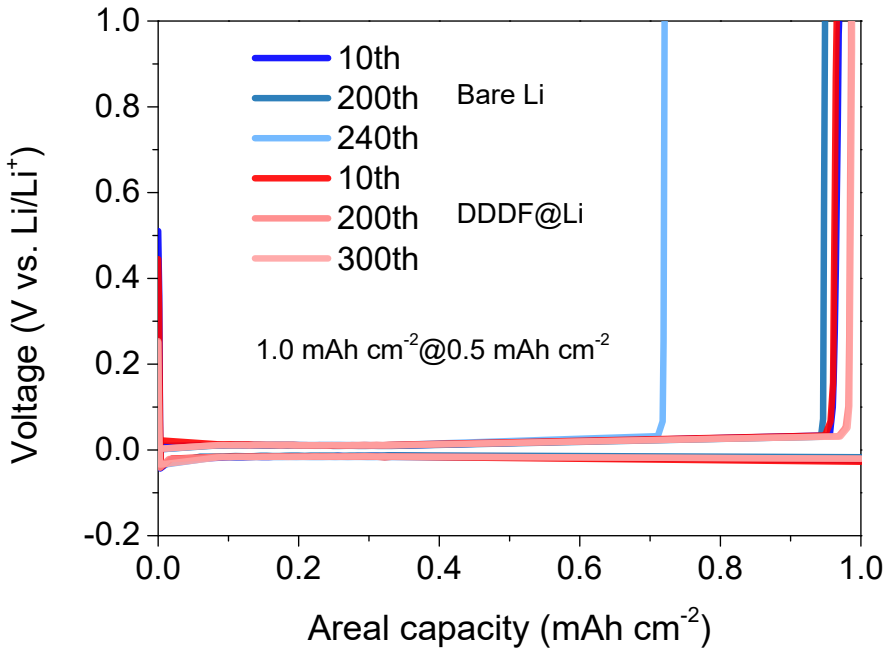

Fig. S6. Time-voltage profiles of Li||Cu cells at 1 mA cm^{-2}-1 h.

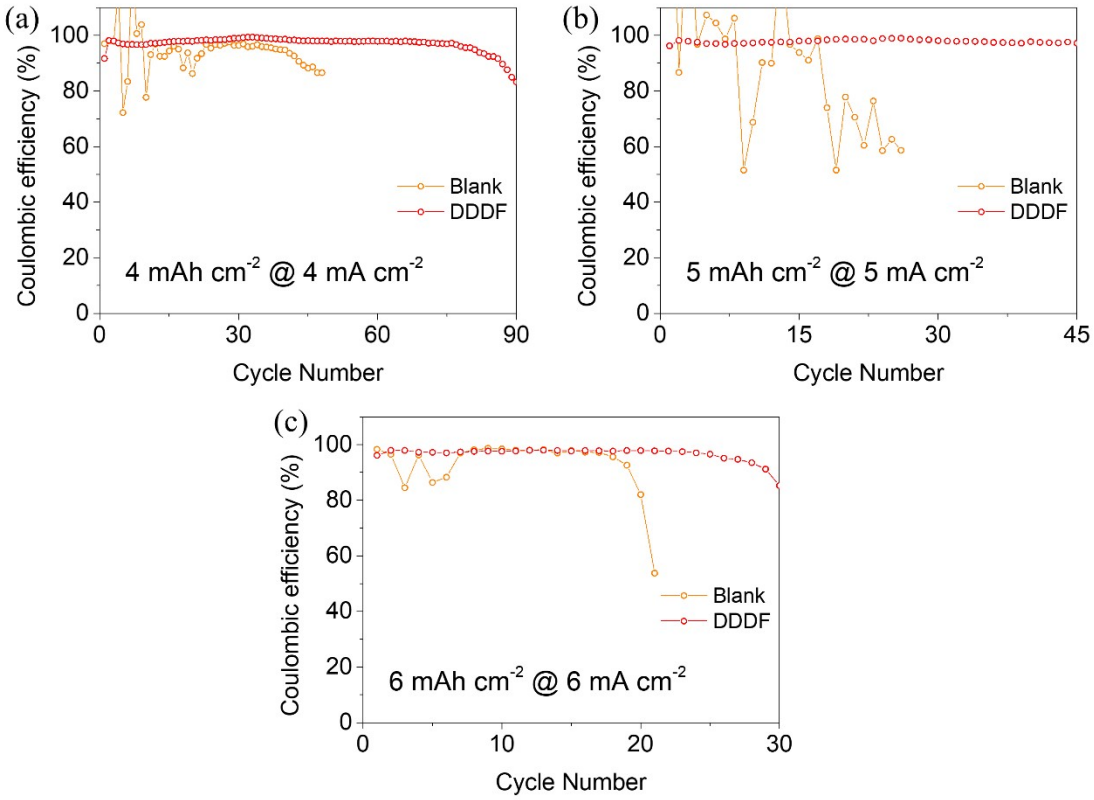

Fig. S7. CE stability over cycling for cells with bare Li and DDDF-Li at higher current density of (a) 4, (b) 5 and (c) 6 mA cm^{-2}.

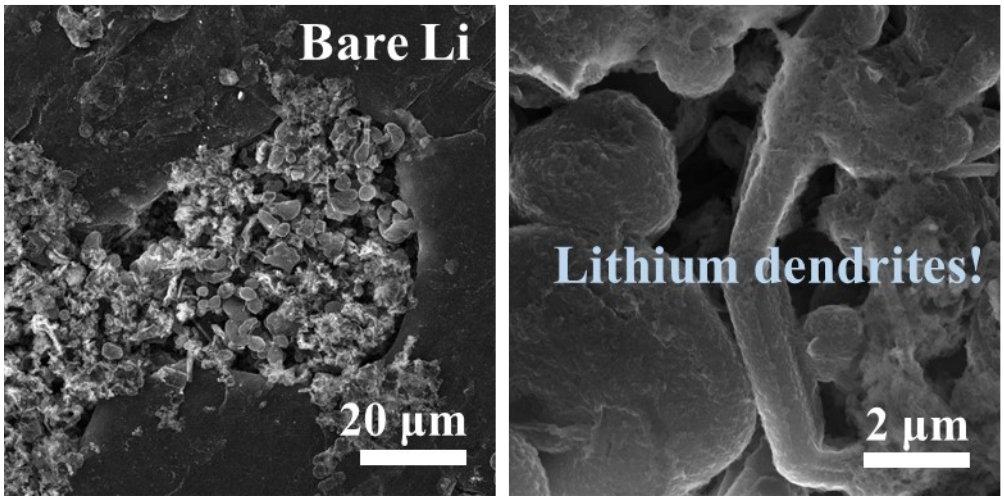

Fig. S8. Morphology evolution of cycled Li metal anodes extracted from bare Li||Cu asymmetrical cells at 1 mA cm^{-2}.

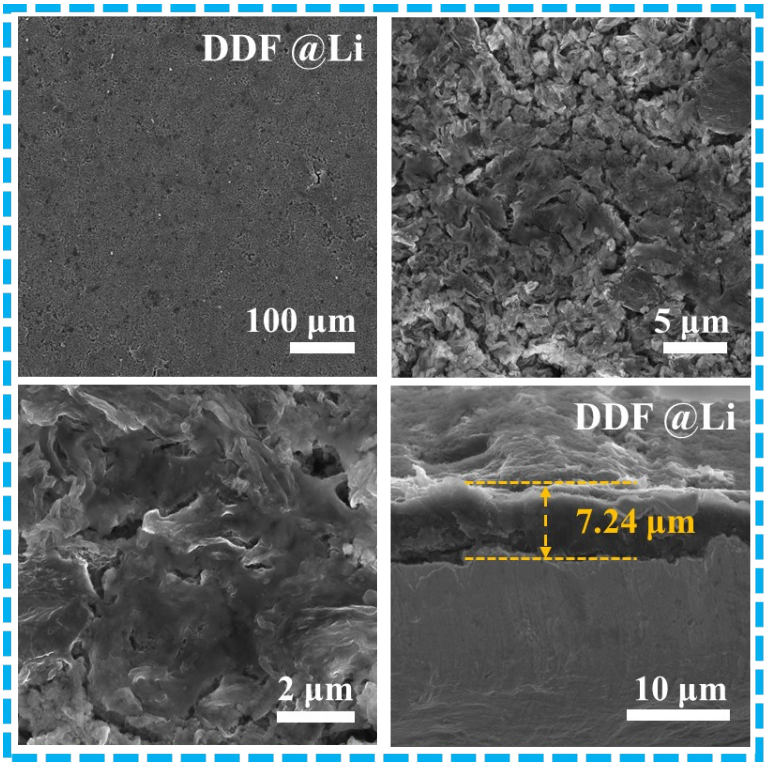

Fig. S9. Morphology evolution of cycled Li metal anodes extracted from modified DDF@Li||Cu asymmetrical cells at 1 mA cm^{-2}.

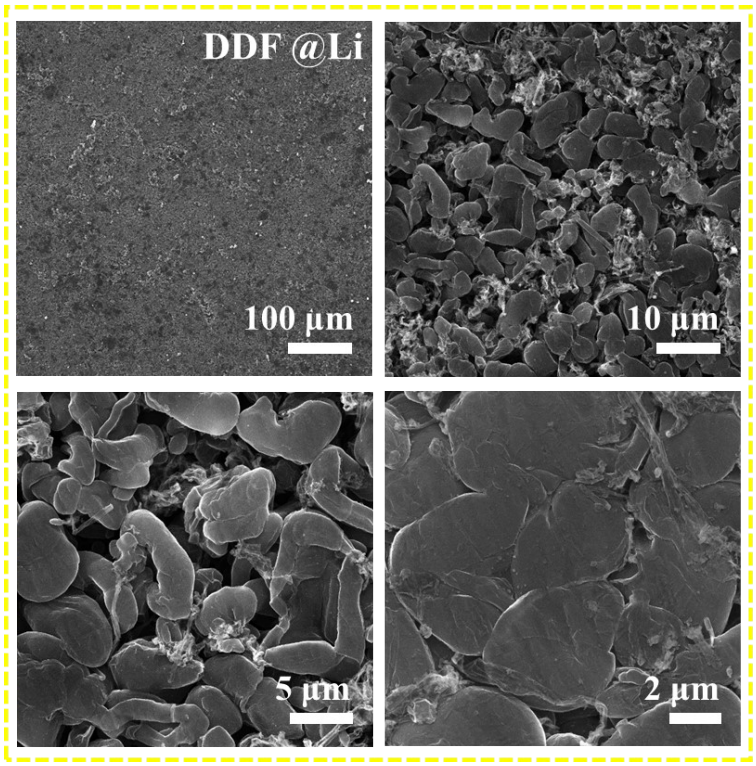

Fig. S10. Morphology evolution of cycled Cu electrodes extracted from modified DDF@Li||Cu asymmetrical cells at 1 mA cm^{-2}.

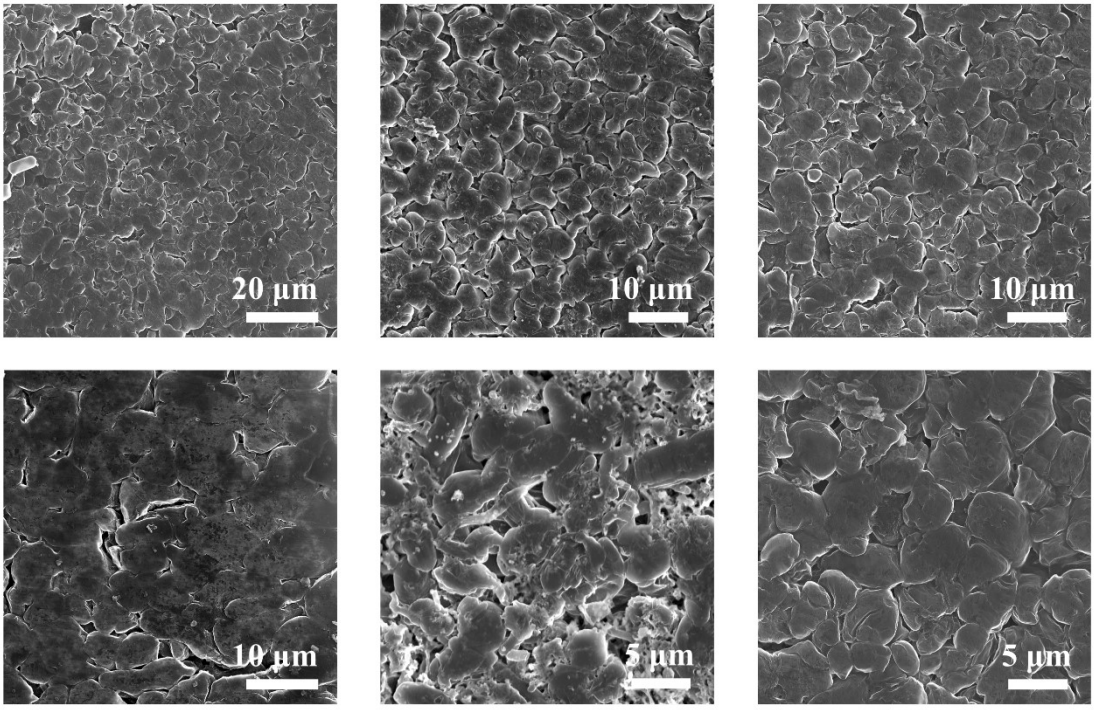

Fig. S11. Top-view SEM images of Li deposition morphology on the Cu substrate with DDDF@Li at different scales.

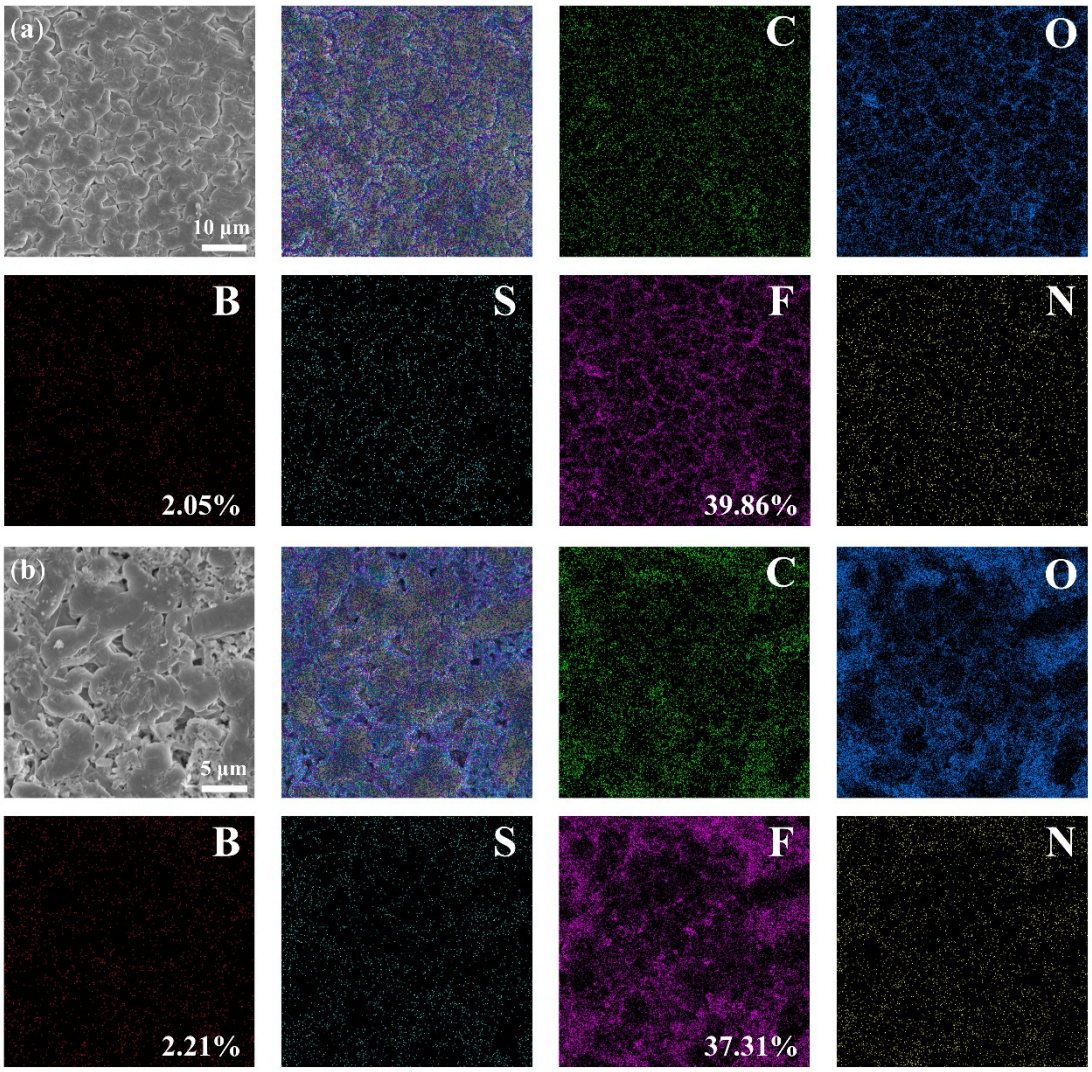

Fig. S12. The SEM image of Li deposition morphology on the Cu substrate with DDDF@Li and corresponding EDS elemental maps for C, O, B, S, F, and N. (a) and (b) refer to different regions selected for testing.

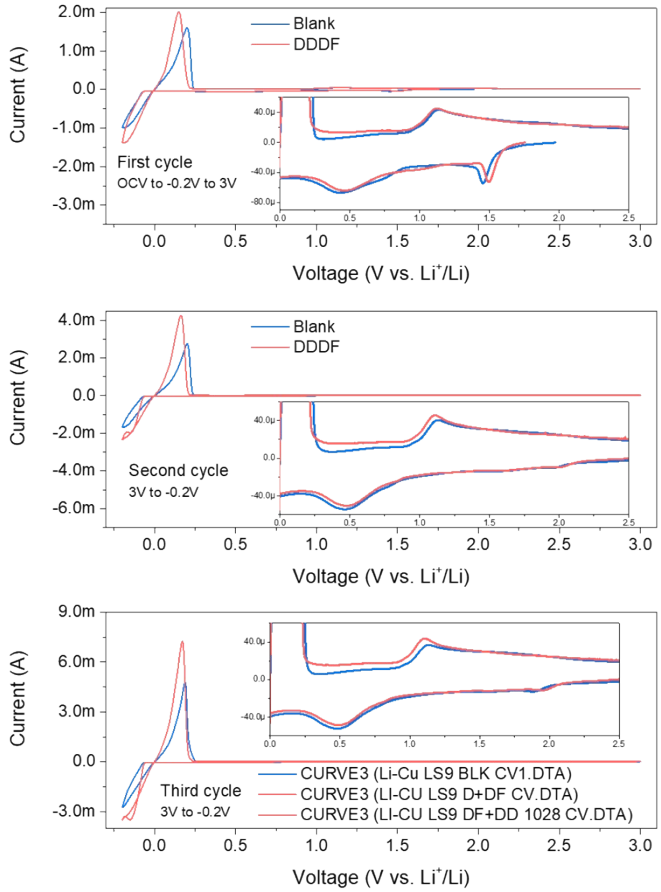

Fig. S13. CV curves of Li-Cu cells with different Li foils at different cycling stage.

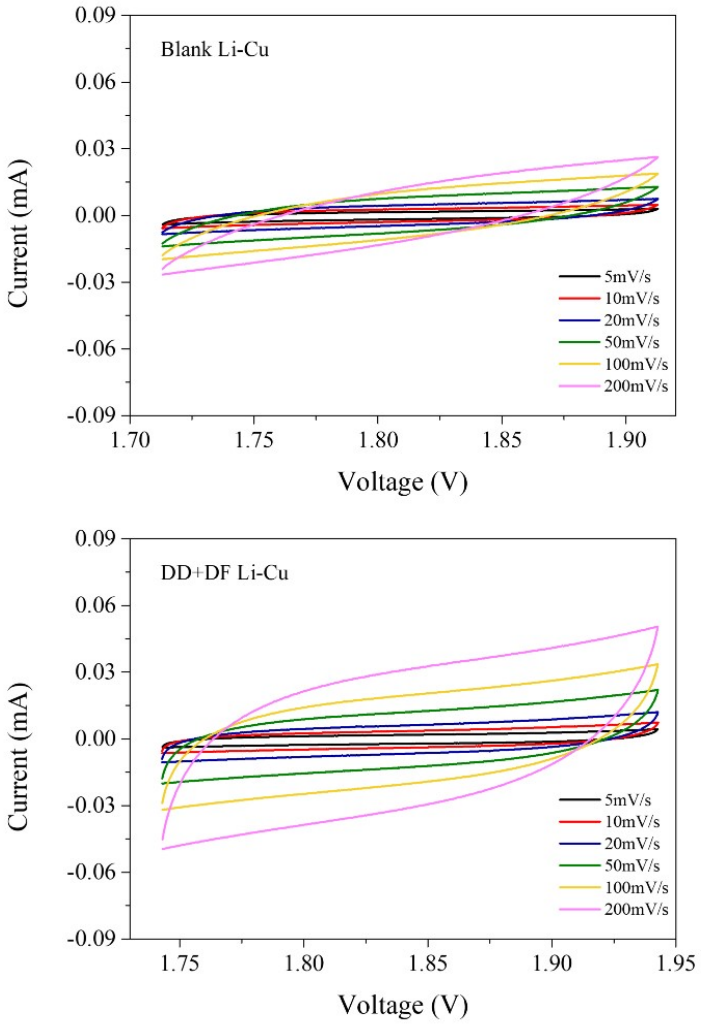

Fig. S14. Electrochemically active surface area (ESCA) of Li-Cu cells measured with different Li foils.

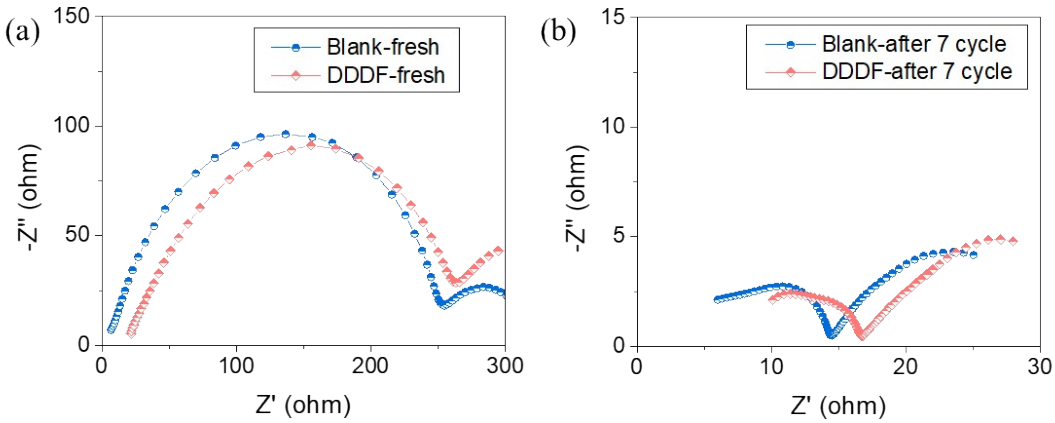

Fig. S15. EIS plots recorded from symmetrical Li||Li cells with different Li foils at different state: (a) fresh cell and (b) cycled cells after 7cycles.

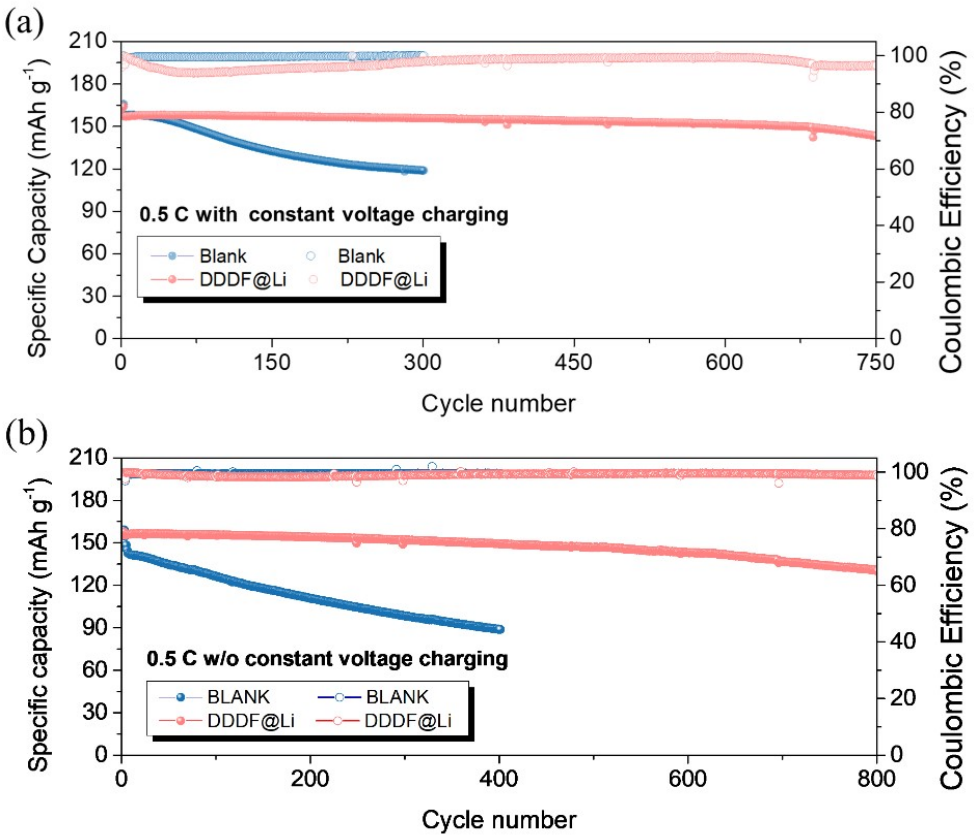

Fig. S16. Long-term cycling performance of Li||LFP full cells a) with and b) without constant voltage charging process at 0.5 C.

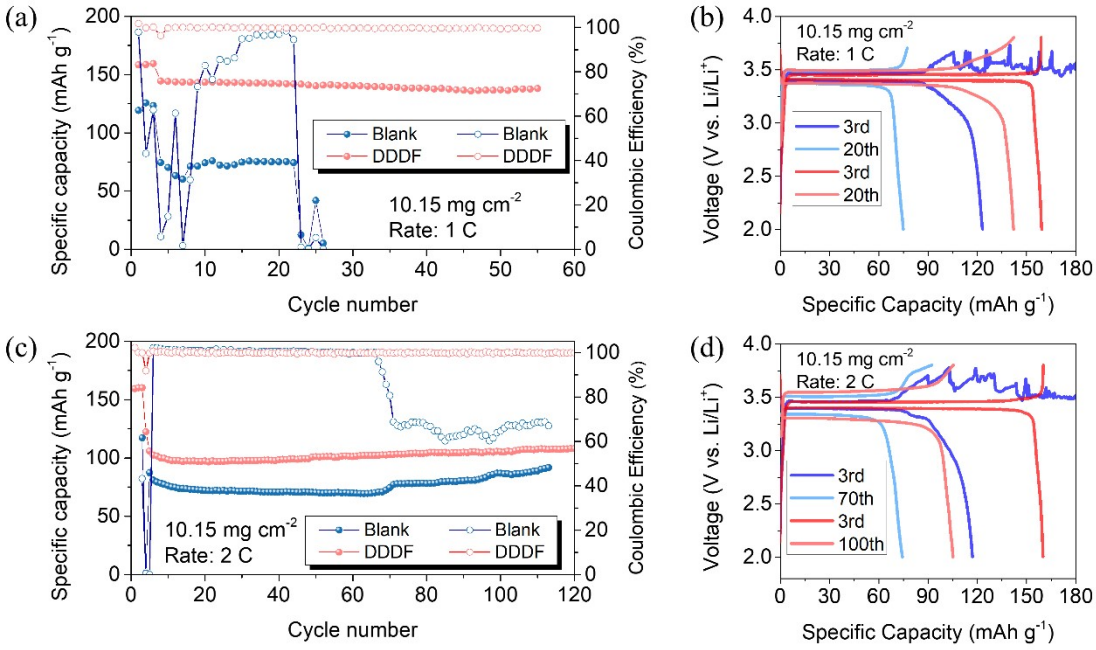

Figure S17. Long-term cycling performance of Li||$LiFePO_4$ full cells using blank and DDDF@Li anodes at (a) 1 C and (c) 2 C with high-loading cathodes. The corresponding charge-discharge voltage profiles of Li||$LiFePO_4$ full cells at (b) 1 C and (d) 2 C at the selected cycles.

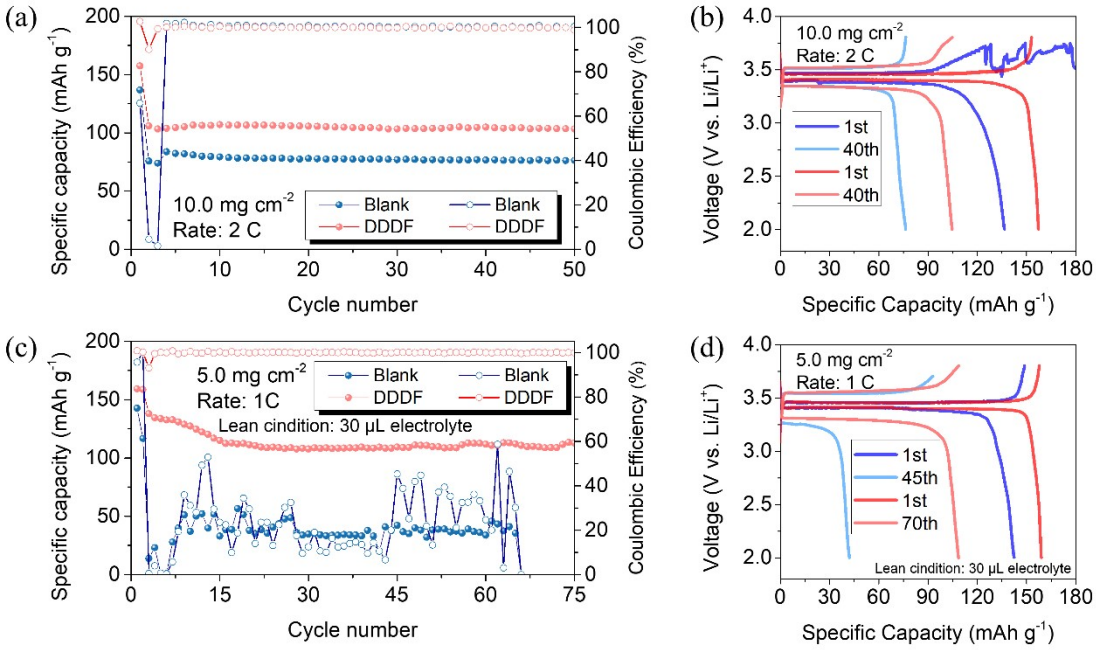

Figure S18. Long-term cycling performance of Li||$LiFePO_4$ full cells using blank and DDDF@Li anodes at (a) 2 C and (c) 1 C with less electrolyte. The corresponding charge-discharge voltage profiles of Li||$LiFePO_4$ full cells at (b) 2 C and (d) 1 C with less electrolyte at the selected cycles.

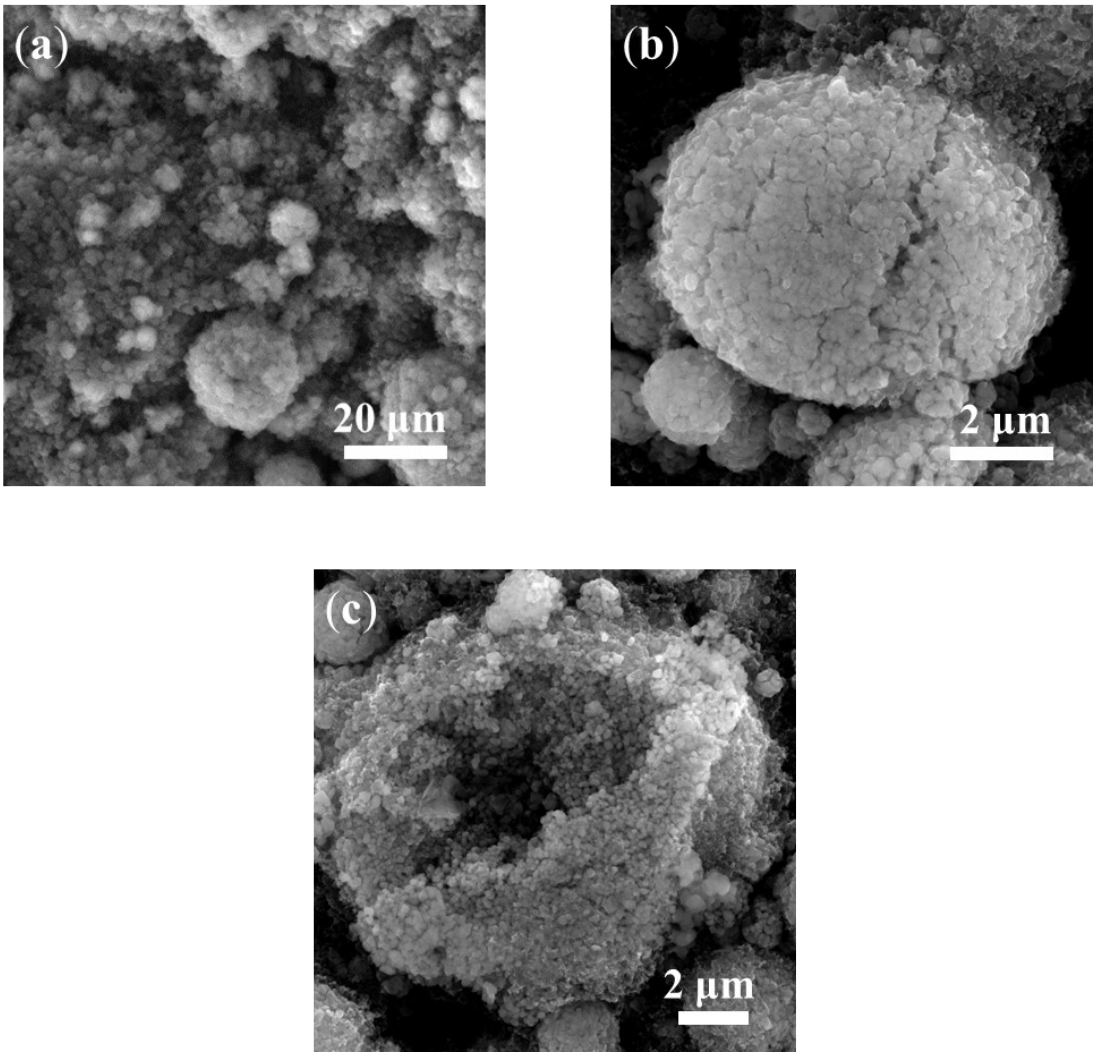

Fig. S19. SEM images of cycled LFP electrodes in pristine Li-LFP cells after long-term cycling. Much clear cracks and more porous morphology with a thick layer can be observed.

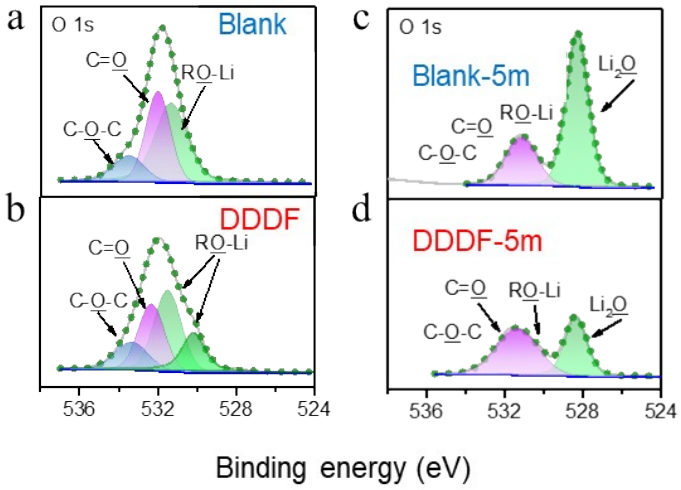

Fig. S20. XPS supplements (surface) of **Figure 8** for cycled Li anodes from Li-Li cells after cycling.

These peaks at 528.2 eV, 531.7 eV, 532.2 eV, and 533.8 eV can be observed in O 1s spectra (**Figure S20**), which are assigned to Li_2O, alkyl lithium (RO-Li, R= alkyl) and Li_2CO_3, C=O, and C-O, respectively. The composition distribution and their relative proportions here are essentially identical to that in the C 1s spectra, in which the C=O and lithium carbonate are the main forms on the surface. Some alkyl lithium also appears owing to the polyether carbon species. After 5 min of etching, the main C-containing components change to the RO-Li, indicating the polymeric feature is present throughout the entire SEI.[2,3] Moreover, an obvious peak of Li_2O arises in the post-etch SEI (528.2 eV). Since lithium oxides are the native species on pristine Li metal, this demonstrates that the metallic Li deposition or pristine Li substrate is exposed after etching.[4,5] This is well consistent with the existence of C-Li in **Figure 8**a. As for the phenomenon of a larger peak in **Figure S20c, d** (Li_2O), this should be considered that the surface species on bare Li are lack diversity with the main form of single lithium oxide.

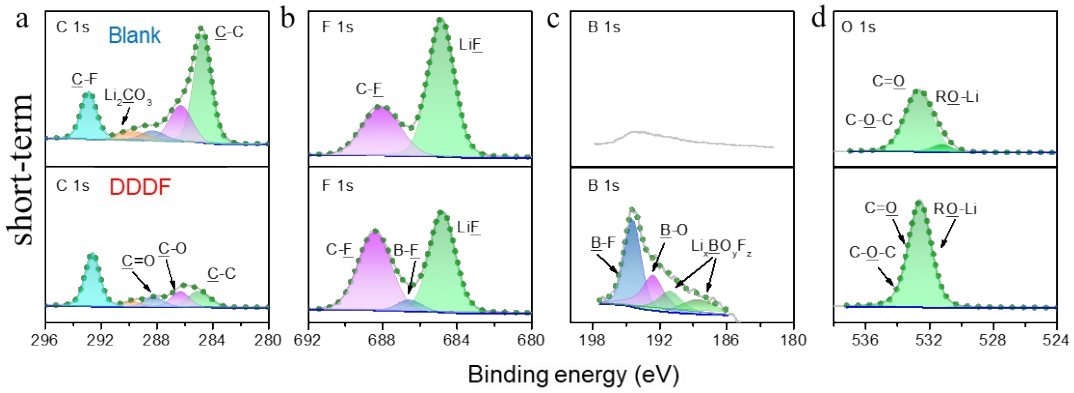

Fig. S21. XPS supplements (surface) of **Figure 8** for cycled Li anodes from Li-LFP cells after short-term cycling.

As shown in **Figure S21**, the detailed SEI information after short cycles on Li metal anode in full cells is presented. Due to different electrochemical windows for various cell configurations, the SEI properties show some subtle differences. Apart from the similar situation shown in Li||Li cells for the C 1s spectra (Figure 8a), more organic fluoride (C-F) species are presented after 10 cycles (**Figure S21a**), which implies a more frequent decomposition reaction in full cells during the initial stage, especially for the DDDF layer.[6] The F 1s and B 1s spectra also can corroborate this behavior with the high peaks of LiF, C-F, and B-F (**Figure S21b, c**). The higher content of B-F species could be attributed to the redundant resource of LiDFOB salt, while the additional peaks in B 1s are the highly decomposed products including B-O polymer and Li-B-O-F species.[7,8] The feature enriching many polymeric compounds of the SEI is illustrated in O 1s spectra (**Figure S21d**). A more obvious peak of the RO-Li and polyether carbon is shown in **Figure S21d**, which indicates more organic phase mostly originating from the decomposition of ether solvents is in the anode surface.[2,3]

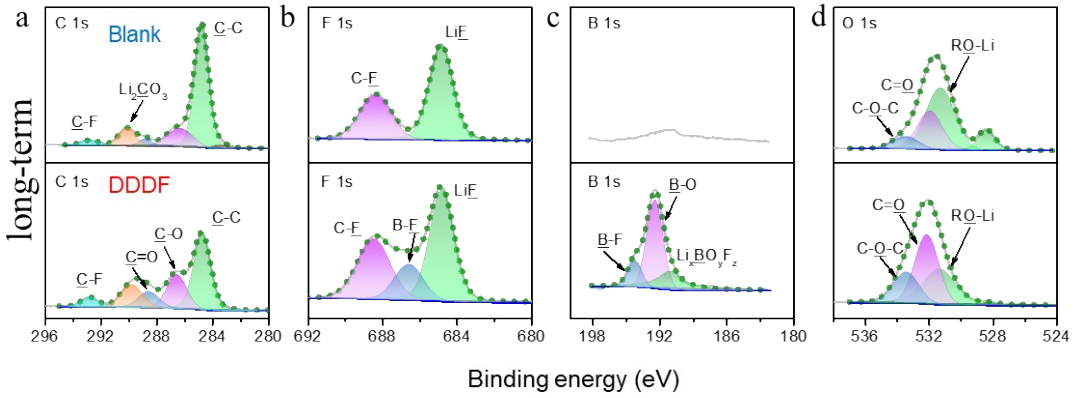

Fig. S22. XPS supplements (surface) of **Figure 8** for cycled Li anodes from Li-LFP cells after long-term cycling.

After hundreds of cycles, the SEI layer should primarily be considered to be a relatively stable interface, thus can better reflect the differences between the modified anode and the bare one. More organics like the dominating C-C peak can be found in the C 1s spectra of the bare Li (**Figure S22a**). Except for a relatively smaller proportion of organic fluoride (C-F) in the long-term cells, the proportion of other species is nearly unchanged both for **Figures S21 and S22**, holding the roughly constant content of these compounds. This also demonstrates the stable SEI layer of the two samples (**Figure S22**). The F-rich SEI in the modified anode can be well maintained even after long-term cycles, as well as the indispensable peak of B-F (**Figure S22**). In addition, an interesting phenomenon can be noticed that the relative maximum intensity of peaks changes from B-F to B-O (**Figures S21c, S22c**). This should be ascribed to the substantial depletion of LiDFOB salt after long circulation and then further produce more B-containing decomposition products. As for the peaks in O 1s spectra (**Figure S22d**), these polymeric compounds (RO-Li, C=O, C-O,) can both be detected, which is well consistent with the previous analysis. While the inappropriate presence of the Li_2O peak may be due to the irregular lithium deposition with a damaged surface.[4]

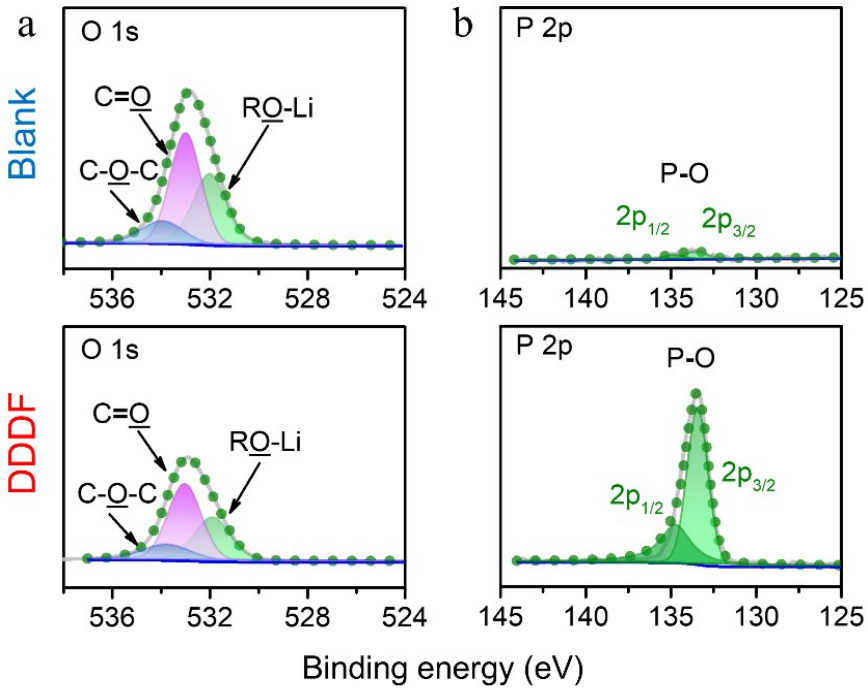

Fig. S23. XPS supplements (surface) of **Figure 8** for cycled LFP cathodes from Li-LFP cells after long-term cycling.

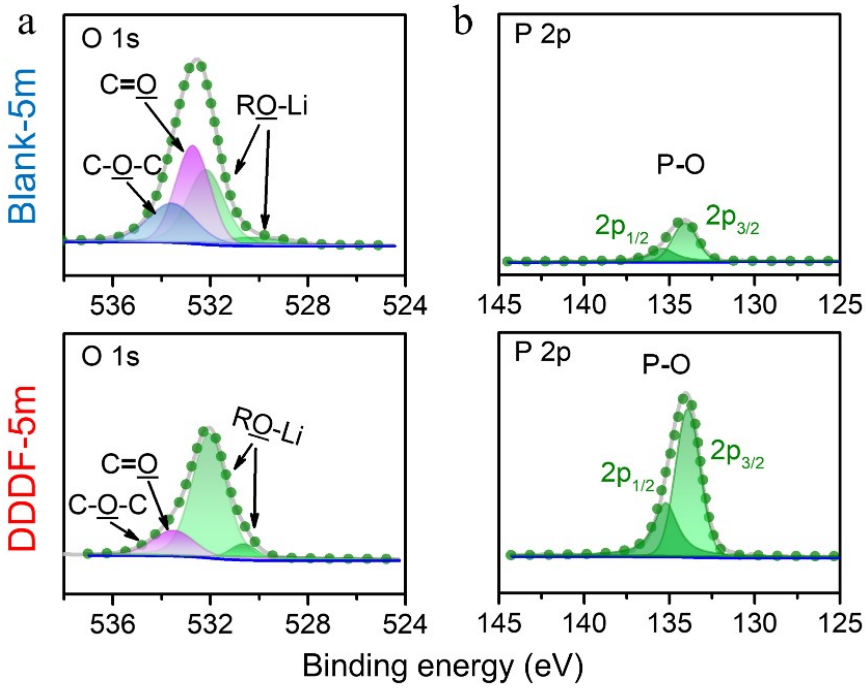

Fig. S24. XPS supplements (inner layer) of **Figure 8** for cycled LFP cathodes from Li-LFP cells after long-term cycling.

The P 2p spectra display common double peaks with positions at 133.8 eV for P $2p_{3/2}$ and 135.0 eV for P $2p_{1/2}$ (**Figures S23b and S24b**), attributed to the P-O bond from phosphate species (PO_4^{3-}).[9-11] The additional peaks of P-F (137.1 and 138.3 eV for P $2p_{3/2}$ and $2p_{1/2}$ respectively) in the CEI of the blank cell are speculated to be the concomitant products that adsorbate on the cathode surface.[7] After etching for the long-term cycling cells, the dominant peaks in P 2p profiles are just the P-O signals of PO_4^{3-}. The weaker signals of the etched P-O bond in blank cells should be the concealment of the heavily covered layer arising from electrolyte decomposition products (**Figure S24b**), as the outer CEI layer shows an almost undetectable signal for PO_4^{3-} (**Figure S23b**).[9,10] In contrast, cells with the DDDF layer display clearer peak shapes of the P-O bond, implying the stable interfacial layer with a relatively thin thickness to facilitate the fast diffusion of Li ions.

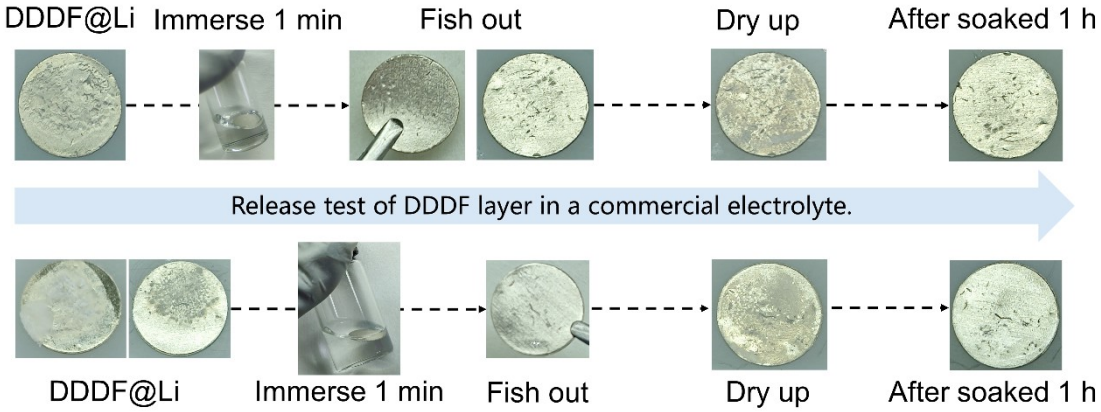

Fig. S25. The measurement of the anion-release behavior of the DDDF layer.

To further confirm the anion-release behavior of this layer, the dissolution test of LiTFSI and LiDFOB from the DDDF layer into a commercial electrolyte was measured in a glass bottle, and experimental details of the sample preparation and anion-release measurement are shown in **Figure S25**. First, the modified Li foils with DDDF layer were prepared and then dropped into the frequently-used commercial electrolyte solutions. Considering the large solubility both of LiTFSI and LiDFOB in ether solution and the potential existence of DOL and DME solvents, the Li foil shows a relatively smooth and shiny morphology just after immersing for 1 min, while the previously visible DDDF layer can be still maintained. However, the thickness of the original coating layer obviously decreases. After the Li foil becomes dry, a thin layer of DDDF component can be seen. When the immersion time is further extended to 60 min, the modified Li can still hold a thinner DDDF layer. In short, the DDDF layer will be thinner after immersion at different times, but the surface of the modified anode will still possess a visible modified DDDF layer. Therefore, pre-plating anions always exist and serve as the natural attributes with a successful anion-release behavior, which can further compensate for the consumption of these favorable anions during cycling. Accordingly, cycling performances can be effectively improved to endow with long-term stability due to the modified lithium foil, while the bare Li will deliver inferior performances as the inhomogeneous SEI film and severe dendritic Li growth as illustrated in **Figure 1a**.

References

1 M. Nie and B. L. Lucht, *J. Electrochem. Soc.*, 2014, 161, A1001.

2 J. Park, S. Ha, J. Y. Jung, J.-H. Hyun, S.-H. Yu, H.-K. Lim, N. D. Kim and Y. S. Yun, *Adv. Sci.*, 2022, 9, 2104145.

3 H. Wu, H. Jia, C. Wang, J.-G. Zhang and W. Xu, *Adv. Energy Mater.*, 2021, 11, 2003092.

4 J. Meng, M. Lei, C. Lai, Q. Wu, Y. Liu and C. Li, *Angew. Chem., Int. Ed.*, 2021, 60, 23256-23266.

5 H. Wang, M. Matsui, H. Kuwata, H. Sonoki, Y. Matsuda, X. Shang, Y. Takeda, O. Yamamoto and N. Imanishi, *Nat. Commun.*, 2017, 8, 15106.

6 W. Li, H. Yao, K. Yan, G. Zheng, Z. Liang, Y.-M. Chiang and Y. Cui, *Nat. Commun.*, 2015, 6, 7436.

7 J.-Y. Liang, X.-D. Zhang, Y. Zhang, L.-B. Huang, M. Yan, Z.-Z. Shen, R. Wen, J. Tang, F. Wang, J.-L. Shi, L.-J. Wan and Y.-G. Guo, *J. Am. Chem. Soc.*, 2021, 143, 16768-16776.

8 S. Li, Q. Liu, W. Zhang, L. Fan, X. Wang, X. Wang, Z. Shen, X. Zang, Y. Zhao, F. Ma and Y. Lu, *Adv. Sci.*, 2021, 8, 2003240.

9 B. Cui, C. Liu, J. Zhang, J. Lu, S. Liu, F. Chen, W. Zhou, G. Qian, Z. Wang, Y. Deng, Y. Chen and W. Hu, *Sci. China Mater.*, 2021, 64, 2710-2718.

10 J. Lin, Y.-H. Sun and X. Lin, *Nano Energy*, 2022, 91, 106655.

11 Q. Peng, Z. Liu, L. Jiang and Q. Wang, *Adv. Energy Mater.*, 2022, 12, 2104021.